KLOE note n. 161
July 1997

# d$E$/d$x$ resolution in a 90%He–10%$i$$C_4H_{10}$ gas mixture with 50 GeV/$c$ pions

G. Finocchiaro,[a] M.Piccolo,[a] P. Valente[b]

[a] Laboratori Nazionali di Frascati dell'INFN, Frascati

[b] Dipartimento di Fisica dell'Università e Sezione INFN, Tor Vergata

## ABSTRACT

The performances of a small size prototype of the KLOE drift chamber (prototype 0.3) in the measurement of specific ionisation are analysed. The data were collected at CERN with a 50 GeV/$c$ pion beam. Using a truncated mean technique, we find a d$E$/d$x$ resolution of 3% with 100 samples. We have investigated the dependence of this result upon several parameters such as the operating voltage, the number and the accepted fraction of collected hits in the truncated mean, etc. The implications for $\pi/\mu$ separation at low momenta are also discussed, with special emphasis to the KLOE environment.

# 1. Introduction

The analysis described in this paper has been performed on data collected in Sep. '94 at the X7 SPS pion beam. The goal of the test was to study the performances, in terms of space-time relations and spatial resolution, of a small prototype with 49 $3 \times 3\,\mathrm{cm}^2$ square cells of the KLOE drift chamber in a magnetic field. A detailed description of the prototype and of the data taking conditions can be found in [1]. We are interested here in studying the performances of our detector in the measurement of specific ionisation. An earlier study of this subject, performed on the $2 \times 2\,\mathrm{cm}^2$ cells prototype 0.1, is contained in [2].

## 1.1 Experimental setup

The sample considered was taken as reference at B=0; out of the 30 read out cells, we used the 25 innermost ones, which have a rather homogeneous gain. The beam, defined by the coincidence of two scintillators, crossed the prototype as it is schematically shown in fig. 1. The analog output from the wires was fed to an ADC with a $3.9\,\mu$s gate, wide enough to collect practically all the ionisation produced by tracks at any distance from the sense wire, as confirmed by the correlation between the total collected charge and the time of arrival of the first electron, shown in fig. 2, in tab. 1, and by the correlation shown in fig. 12.

| time cut (ns) | Events/Total |
|---|---|
| 1,000 | 0.89 |
| 1,500 | 0.94 |
| 2,000 | 0.96 |
| 4,000 | 1.00 |

**Tab. 1:** *Percentage of events with the first electron arriving before a given time cut.*

## 1.2 Quality cuts and data sample

A typical raw ADC spectrum is shown in fig. 3. The pedestal presents a gaussian shape: its mean value is subtracted in the following; the nominal ADC conversion factor is 0.25 pC/ch. A cell is defined as 'hit' if its ADC reading (pedestal subtracted) is bigger than 3 times the pedestal width. The multiplicity of hit cells is shown in fig. 4; values bigger than 5 are mostly due to tracks at the boundary between two cells releasing a measurable signal in both of them, while the tail on the low side is due to small cell inefficiencies.

The data sample analysed and the corresponding prototype operating voltages and number of events are summarised in tab. 2.

| HV (V) | Run # | # of events ($\times 10^3$) |
|---|---|---|
| 1,750 | 111 | 10 |
| 1,800 | 110 | 10 |
| 1,850 | 96/99/107b* | 50/50/10 |
| 1,900 | 108/158/163 | 10/50/50 |
| 1,950 | 109 | 10 |

**Tab. 2:** *Summary of the analysed data samples.*

We select a clean sample of events for the subsequent analysis by furtherly applying the following cuts:

1. $N_{\text{HITS}} \geqslant 4$, to select a good track ($\varepsilon$=83.8%).
2. $R_{\text{drift}} \leqslant 1.5\,\text{cm}$ ($\varepsilon$=87.3%).
3. One and only one cell hit per layer ($\varepsilon$=93.1%).

The combined efficiency of the above cuts is about 79%.

No provision was made to take into account ADC's channel-to-channel conversion differences (order of few percent). The differences in the gas amplification among the various cells are roughly of the same magnitude, given the cell geometry and the tolerances on the diameter and positioning of the wires. A last source of inhomogeneity, of the order of 10%, is expected to come from the amplifiers.

We performed a cell intercalibration by determining the most probable (MP) value of each pulse height distribution.[(1)] Distributions of the fitted MP values are shown in fig. 5, for each cell used, and at different operating voltages. The single charge measurements are then recalibrated scaling them by the factor $\text{MP}_i/\langle\text{MP}\rangle$, where $\text{MP}_i$ is the most probable value of the $i$-th cell, and $\langle\text{MP}\rangle$ the average of the same quantity over all the cells (fig. 6).

# 2. Results

## 2.1 The Truncated Mean technique

The limitation due to the large fluctuations, in thin materials, of the single $\mathrm{d}E/\mathrm{d}x$ measurements around the most probable value, can be drastically reduced by sampling

* We named '107b' the run collected after run # 107, which by mistake had been labeled as 'run 1'.

(1) A gaussian fit centered around the mean value of the distribution and extended to ± its R.M.S. is rather accurate: the fitted value is very stable against small changes of the limits of the fit.

several times the specific ionisation along each track. Because of the Landau tails, the improvement is less than the $1/\sqrt{n}$ factor one would expect from pure Poisson statistics, but still of the same order of magnitude.

The Truncated Mean (TM) technique is often used to eliminate, or at least reduce, the effect of the high energy tail of the $\mathrm{d}E/\mathrm{d}x$ distribution. It essentially consists in discarding the hits of a given track with the highest $\mathrm{d}E/\mathrm{d}x$, under the assumption that they belong to the Landau tail. The average of the remaining hits should then be a good estimate of the 'true' specific ionisation. As we have seen before, the average multiplicity in our setup is about 5 hits. This figure is of course not high enough to reach resolutions relevant for typical particle identification requirements. However, since the momentum spread of the beam was very low (and in any case at 50 GeV/$c$ it would be irrelevant) we can accumulate hits belonging to different events to form fake tracks $\mathcal{N}$ hits long, out of which a fraction $f_{\mathrm{acc}}$ is accepted.

On the same footing we can safely neglect the difference in specific ionisation due to the possible contamination of particle species other than pions in the beam. Finally, since we are dealing with square cells and the beam divergence was less than 2 mrad, no track length corrections has to be applied.

Examples of TM distributions for few values of $\mathcal{N}$ ($50 \leqslant \mathcal{N} \leqslant 100$) and of the accepted fraction of hits ($f_{\mathrm{acc}}$=0.75, 0.95) are shown in fig. 7. Gaussian fits are superimposed to the histograms; comparing the R.M.S. of the distribution and the sigma of the gaussian fit, one actually sees that the tails are in fact drastically reduced with respect to the single pulse height distribution of fig. 3. The effect of averaging several measurements is also evident: the 25% resolution of the single measurement reduces to about 3.2% with $\mathcal{N}$=100. The behaviour of the resolution in the TM vs. number of samples (after truncation) can be seen in fig. 8, with HV=1,850 V and $f_{\mathrm{acc}}$=80%. The expected $1/\sqrt{n}$ scaling behaviour is observed.

### 2.2 Linearity of the TM measurement

In this section we study the impact of the saturation of the pulse height measurements on the $\mathrm{d}E/\mathrm{d}x$ resolution. Saturation effects can originate from two distinct causes, namely the non linearity of the ADC and of the gas amplification. Both phenomena can result in an artificial reduction of the Landau tails. In the first case, the high part of the spectrum is simply cut out. The second effect is more subtle: at very big gains, the large charge at the anode could decrease the effective amplification, again reducing the tails.

We show in fig. 9 the pulse height distributions for several operating voltages. The saturation of the ADC scale, and its effect on the (apparent) resolution of the charge measurement, are clear. The ratio between width and most probable value of the peak, amounting, as quoted above, to about 25%, depends only very weakly on the operating voltage. This parameter on the contrary affects the ratio *R.M.S./Mean*, which ranges from 56% at HV=1,750 V to about 24% at HV=1,900 V, where the Landau tails are in fact cut out.

The cutting off of the tails in the single cells amplitude produces a clear effect on the truncated mean. This can be observed in fig. 10, where $\sigma_{\mathrm{d}E/\mathrm{d}x} \equiv \sigma(\mathrm{d}E/\mathrm{d}x)/\langle \mathrm{d}E/\mathrm{d}x \rangle$ from the TM distributions is shown as a function of $f_{\mathrm{acc}}$, for four different $\mathcal{N}$ choices, and for operating voltages ranging from 1,750 to 1,900 Volts. The last plot of this figure (HV=1,900 V), where no dependence on the fraction of accepted hits is observed, is a direct consequence of the cutting off of the corresponding pulse height distribution of fig. 9.

On the contrary, a broad minimum is found in the plots of fig. 10 corresponding to lower operating voltages, where a sort of optimisation can be found as a function of the truncating fraction.

In order to investigate a possible gas gain saturation, we have studied how the MP pulse height varies with the high voltage.(2) The points representing the most probable values(3) are fitted separately in fig. 11 in the 'low' and in the 'high' HV regime: we find the same slope, within the errors, in the two cases. In other words, the data do not support the hypothesis of a gas gain saturation, which would be signaled by a less steep slope in the 'high' HV region.

Saturation could also show up by a decrease of the collected charge with the drift distance: the ionisation clusters are more grouped in time to the anode if they originate from distant tracks, therefore a gas gain saturation would be more likely in this situation.

In fig. 12 the MP value is plotted, as a function of the drift distance, for the different voltages. Straight line fits, performed excluding small and big drift radii, to avoid effects due to $t_0$ misassignments and drift field inhomogeneities, are superimposed to the curves. The linear coefficient is compatible with zero (but there are sizeable fluctuations due to the limited statistics) at HV=1,750 and 1,800 V, and becomes negative at the two highest tensions. However, at 1,900 V the effect amounts only to 3%: for this reason, even if in

(2) As it is seen from fig. 5, in the data sample collected at the highest voltage (1,950 V), the gas gain in several cells was so high that not only the tails were cut, but even the MP values were above the ADC full scale, causing the failure of the fit which determines the MP value itself. For this reason it was not possible to extend the TM analysis to the 1,950 V data. On the contrary, the few cells where the pulse height peak happened to lay within the range of the ADC could be used in the 'gas gain saturation' study.

(3) We have assigned to the MP values error bars obtained adding in quadrature the statistical error from MINUIT [3] and a 'systematic uncertainty', estimated from the spread in the MP value observed comparing several runs taken exactly in the same conditions.

principle any dependence of the pulse height with the drift distance can be corrected for, we decided it was not worth doing it in this case.

It has to be stressed that the above result is actually an upper limit for gas saturation: a decrease of the collected charge with the impact parameter can in fact be also due to the finite integration gate (the latter was in our case 3.9 $\mu$s, wide compared with typical electron drift times), or to the presence of electronegative agents in the mixture.

In fig. 13 the d$E$/d$x$ resolution vs. the prototype's operating voltage is shown. According to what we have stressed in the present section, the resolution decrease at 1,900 V is to be considered fictitious, and due to the ADC saturation. Since there are only four HV settings, it is hard to draw conclusions upon the other points: the two measurements at 1,800 and 1,850 V seem to belong to a sort of plateau, while the slight resolution deterioration at 1,750 V could be attributed to some amplification fluctuations.

To conclude, we believe that the d$E$/d$x$ measurements performed at 1,800 and 1,850 V (essentially equivalent) are rather realistic: we will refer to them, assuming $f_{\rm acc}$=80%, in the following.

## 3. Extrapolation to low momenta

The specific ionisation measurement can be used to help discriminating different particle species. In particular, in KLOE it is crucial to reach a rejection factor of about $5{\cdot}10^{-5}$ of the $K_{\mu3}$ decay respect to the $K_{\rm L}{\to}\pi^+\pi^-$ one. Much of this factor can be obtained via kinematical cuts [4]; however, it is clear that the help from independent methods is welcome.

Our resolution figure with $\mathcal{N}$=100 and $f_{\rm acc}$=80%, $\sigma^{100}_{{\rm d}E/{\rm d}x}$ = 3.0%, has to be compared with the same number, quoted in [5] as goal for the *cluster counting* method. The latter technique was subsequently abandoned in KLOE because difficult, expensive, and extremely heavy for the DAQ system.

The test beam result has to be properly scaled to the KLOE conditions. First of all, the actual number of hits: we have shown in fig. 8 that the scaling law is essentially $\mathcal{N}^{-0.5}$.

| Particle | $\langle\mathcal{N}\rangle$ |
|---|---|
| $\pi$ from $K_{\rm L}{\to}\pi^+\pi^-$ | 55 |
| $\pi$ from $K_{\rm S}{\to}\pi^+\pi^-$ | 74 |
| $\pi/\mu$ from $K_{\rm L}{\to}\pi\mu\nu$ | 75/92 |

**Tab. 3:** *Average hit multiplicities from not decayed particles in the KLOE drift chamber.*

The average hit multiplicities in the drift chamber are listed in the tab. 3 above [6]. Since the detection of a pion decay, which can be done with high efficiency in KLOE, automatically solves the problem of $\pi/\mu$ discrimination, only stable pions are considered. The correct number to use depends of course on the specific physics channel: to fix the ideas we will consider $\langle\mathcal{N}\rangle$=75 in the following.

The second important point is the different specific ionisation, which in a gas counter can be parametrised by the product $n_{\rm p}(\beta)\cdot N_e(\beta)$. The number of primary clusters $n_{\rm p}$ bears most of the energy dependence of the $\mathrm{d}E/\mathrm{d}x$ curve, while $N_e$ is to some extent insensitive to the energy of the primary particle. Since the statistical distribution of the primary ionisation acts $n_{\rm p}$ is strictly poissonian (with fluctuations $1/\sqrt{n_{\rm p}}$), not a big error is done assuming that also $\sigma_{\mathrm{d}E/\mathrm{d}x}\sim 1/\sqrt{\mathrm{d}E/\mathrm{d}x}$.

From the operative point of view, one has first to accomplish a *specific ionisation* measurement, *i.e.*: 1) normalise the collected charge to unit track length; and 2) relate it to the particle momentum: the $\mathrm{d}E/\mathrm{d}x$ measurement will be subsequent to the track fit. Both operations were of course unnecessary in the test beam data analysis.

Curves of the most probable energy release $\varepsilon_{\rm MP}$ for pions and muons are shown in fig. 14 as a function of the particle's momentum [7]. The curves, referring to our gas mixture 90%He$-$10%$i$C$_4$H$_{10}$, are normalised to their minimum value $\varepsilon_{\rm MIP}$. The use of MP values instead of the average $\mathrm{d}E/\mathrm{d}x$ is not only mandatory, since this is what we measured experimentally, but also allows for a twofold advantage. First, from the point of view of the calculations, one needs not to care about the maximum transferred energy, which affects the tails and hence the average energy loss, but not the most probable value. Secondly, and more important, the curves have their minimum at $\beta\gamma\simeq 3.5$, and not $\beta\gamma\simeq 3.2$ as it happens with the *average* energy loss: this is a bonus for $\pi/\mu$ separation at momenta *below* the minimum, as it is the case for KLOE.

We have to mention that the description of the curve $\varepsilon_{\rm MP}$ vs. $\beta\gamma$ is not unique: using another model [8] for the density correction we find $\varepsilon_{\rm PLATEAU}/\varepsilon_{\rm MIP}\simeq 1.32$ instead of 1.4 as in fig. 14, while coding the formula in [9] using the density corrections and the atomic data published in [10], we find $\varepsilon_{\rm PLATEAU}/\varepsilon_{\rm MIP}\simeq 1.22$, with $(\beta\gamma)_{\rm MIP}\simeq 4.75$. For what we have stated above, the curves of fig. 14, which we have used in the following considerations, set a lower limit to the power of the TM analysis for $\pi/\mu$ discrimination.

In fig. 15 $\mathrm{d}E/\mathrm{d}x$ distributions for $\pi$ and $\mu$ at $p=200\,\mathrm{MeV}/c$ are shown, extrapolated from the measured value $\sigma^{75}_{\mathrm{d}E/\mathrm{d}x}$=3.5% at $50\,\mathrm{GeV}/c$ through the curves of fig. 14. The gaussian shape assumed is justified by the result previously shown in fig. 7. The common area measures the confusion probability between the two particle species. Fig. 16 shows the number of standard deviations separating the pion and the muon peaks, while the pion and muon efficiencies, after a cut in the TM signal exactly at halfway between the two peaks are shown in fig. 17, as a function of the particle momentum. The same figure shows also the rejection factor ($\mathcal{R}_j \equiv \varepsilon_\mu/\varepsilon_\pi$) achievable with such a cut.

One has to mention that only a small number of cells entered the truncated mean in the prototype, whereas in the KLOE chamber there will be 12,000 cells; such figure would imply bigger gain inhomogeneities. However, we have shown not only that the channel-to-channel differences are much smaller than the intrinsic $\mathrm{d}E/\mathrm{d}x$ width, but that the cell gains can be equalised.

### 3.1 Resolution vs. sample thickness

In the KLOE drift chamber we will not have a one-to-one correspondence between ADC channels and sense wires: the latter will be added analogically in groups of 12. We tried to investigate how this could modify our results by simulating analog sums of 5 wires, arranged both orthogonal (in what we define a 'row' of wires) and parallel (in a 'column') to the beam direction. In the first case only one out of the five wires of the row has a signal above pedestal, while in the second case all the five cells of the column are hit. The first case is more realistic: given the quoted hit multiplicities and the total number of cells, the probability to have more than one hit cell inside a group of 12 should not be high. In any case, we recommend that these considerations enter in the choice of the cell grouping.

As expected, when the 'row analog sums' are used in the truncated mean, nothing changes with respect to what described in the past chapter.

On the contrary, the 'column analog sums' should have a threefold effect. First of all, the 'sorting granularity' is reduced, in the sense that the original 100 hits are grouped in 20 super-hits, whose ordering, necessary for the TM, is coarser. On top of this, there are two competing effects: namely the reduced sampling frequency and the increased track length. Their consequences on the relative $\mathrm{d}E/\mathrm{d}x$ resolution have been parametrised in [11] as $\sigma_{\mathrm{d}E/\mathrm{d}x} \propto \mathcal{N}^a \cdot x^b$, with $a = -0.46$, $b = -0.32$ for Argon. This formula would imply the ratio of the $\mathrm{d}E/\mathrm{d}x$ resolution from the 'five cells TM' to the 'single cell TM' to be $\sigma_5/\sigma_1 = 5^{0.46-0.32} = 1.25$, while we observe $\sigma_5/\sigma_1 \simeq 1.1$.

We can measure the $a$ and $b$ coefficients from the data. As it is shown in fig. 8, $a = -0.49 \pm 0.01$. To measure $b$, we simulated 'supercells' of increasing length. The relative width vs. the size of the supercell is plotted in fig. 18: we obtain the value $b = -0.40 \pm 0.01$. Finally, we determine the difference $a - b$ from the TM resolution of the supercells (in this case both the track length and the sampling frequency are important): as it is seen in fig. 19, the result is $a - b = 0.07 \pm 0.01$, consistent, within the errors, with the separate determinations of $a$ and $b$.

We want to stress that this result can be interpreted as a consequence of the small value of the cluster multiplicity and of the limited Landau tails in Helium: the difference between the $a$ and $b$ exponents is to some extent a measurement of skewness of the energy loss distribution: in a completely symmetric distribution the two effects of decreasing the number of samples and increasing the sample thickness would balance out.

## 4. Conclusions

Measurement of specific ionisation in Helium based gas mixture can yield a resolution as good as 3.5% with about 70 samples, 3 cm long. Such a figure is relevant in the KLOE environment to obtain $\pi/\mu$ discrimination for the $\mathcal{CP}$-violating decay $K_{\rm L}\to\pi^+\pi^-$.

We believe that a more complete study of the $\mathrm{d}E/\mathrm{d}x$ resolution, especially in the $1/\beta^2$ region is in order, to explore the experimental possibilities of such technique. The "quasi gaussian" shape of the energy loss distribution in Helium offers very interesting experimental possibilities both in the low and in the intermediate momentum ranges.

## ACKNOWLEDGEMENTS

We would like to thank Dr. Jim Smith from Colorado University for fruitful discussions on the subject.

## FIGURE CAPTIONS

1. Schematics of the beam test layout.
2. Total collected charge vs. arrival time of the first electron.
3. A typical raw ADC spectrum. The operating voltage was 1,800 V.
4. Multiplicity of hit cells.
5. Most probable values of the pulse height distribution in the cells used in the TM analysis.
6. Histogram of the cells' most probable pulse height for several operating voltages.
7. Examples of Truncated Mean distributions for different values of $\mathcal{N}$ and $f_{\rm acc}$; a) $\mathcal{N}$=50, $f_{\rm acc}$=75%; b) $\mathcal{N}$=50, $f_{\rm acc}$=95%; c) $\mathcal{N}$=100, $f_{\rm acc}$=75%; d) $\mathcal{N}$=100, $f_{\rm acc}$=95%.
8. $\mathrm{d}E/\mathrm{d}x$ resolution vs. number of hits used in the truncated mean, in the case HV=1,850 V, $f_{\rm acc}$=80%.
9. ADC spectra (pedestal subtracted) for several operating voltages.
10. $\mathrm{d}E/\mathrm{d}x$ resolution vs. $f_{\rm acc}$ for different $\mathcal{N}$ values and operating voltages.
11. Most probable value of the pulse height distribution vs. operating voltage.
12. Profile of collected charge vs. drift distance.
13. $\mathrm{d}E/\mathrm{d}x$ resolution vs. operating voltage.
14. $\mathrm{d}E/\mathrm{d}x$ curves in 90%He$-$10%$i\mathrm{C_4H_{10}}$.
15. Calculated shapes of the TM distribution at $p = 200\,\mathrm{MeV}/c$.

16. Number of R.M.S. separating the muon and the pion peaks.
17. Pion and muon efficiencies and rejection factor cutting the TM signal exactly halfway between the two peaks.
18. Relative width of the single supercell pulse height distributions, as a function of the supercell length.
19. TM resolution vs. supercell length.

## REFERENCES


1. C. Avanzini *et al.*, *The test of the prototype 0.3 of the KLOE chamber in magnetic field. The measurements at the X7 beam of the CERN West Area*, KLOE note n. 148 (May 1995).
2. M. Pollack, *Energy Loss Measurements in Prototype 0.1*, KLOE note n. 85 (Jan. 1994).
3. F. James, `MINUIT` - *Function Minimization and Error Analysis*, CERN program library entry D506.
4. The KLOE Collaboration, *The KLOE Central Central Drift Chamber, Addendum to the Technical Proposal*, LNF-028/1994 (1994).
5. The KLOE Collaboration, *A general purpose detector for* DAΦNE, LNF-019/1992 (1992).
6. A. Andryakov, private communication.
7. J. Vav'ra *et al.*, *Energy loss measurement in a jet chamber* **NIM203**, 109 (1982), A.H. Walenta, BNL Report, BNL-28328 (1980).
8. R. Ehrlich *et al.*, *Particle identification...* **NIM211**, 17 (1983).
9. A.H. Walenta, *Performance and Development of* $\mathrm{d}E/\mathrm{d}x$ *counters,* Physica Scripta **23**, 354 (1981).
10. R.M. Sternheimer *et al.*, *The Density Effect for the Ionization Loss of Charged Particles in Various Substances,* Atomic Data & Nuclear Data Tables **30**, 261 (1984).
11. W.W.M. Allison and J.H. Cobb, *Relativistic Charged Particle Identification By Energy loss,* Ann. Rev. Nucl. Part. Sci. **30**, 253 (1980).

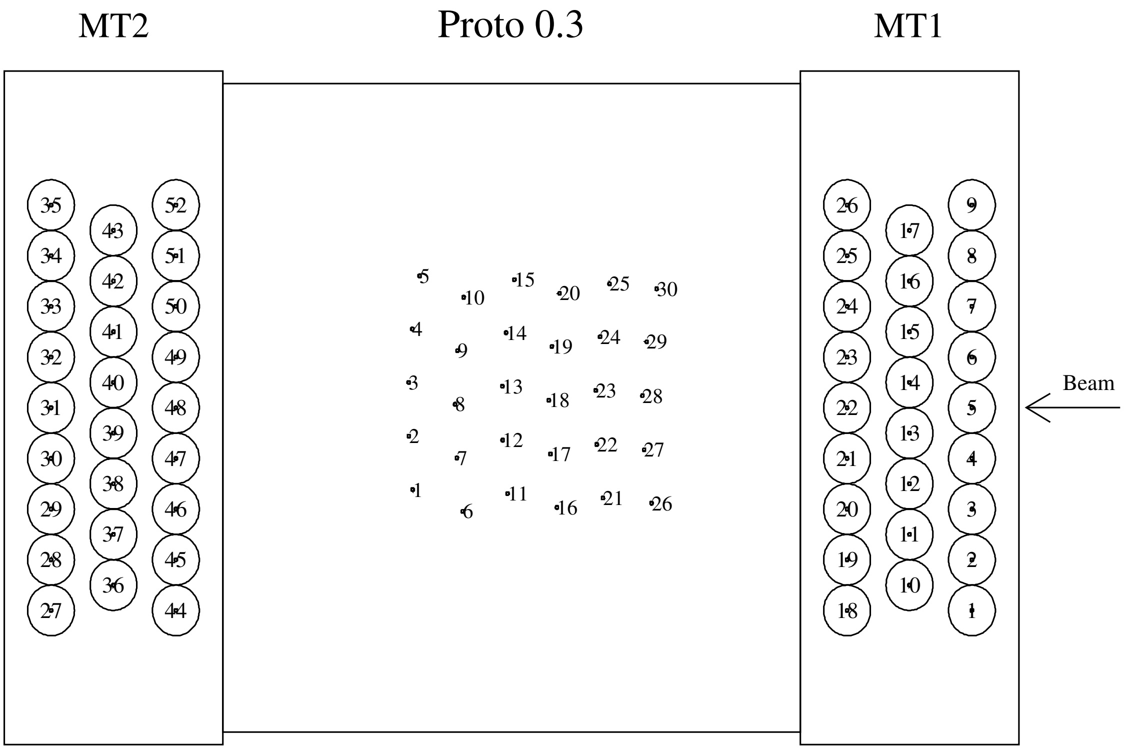


**Fig. 1:** *Schematics of the beam test layout.*

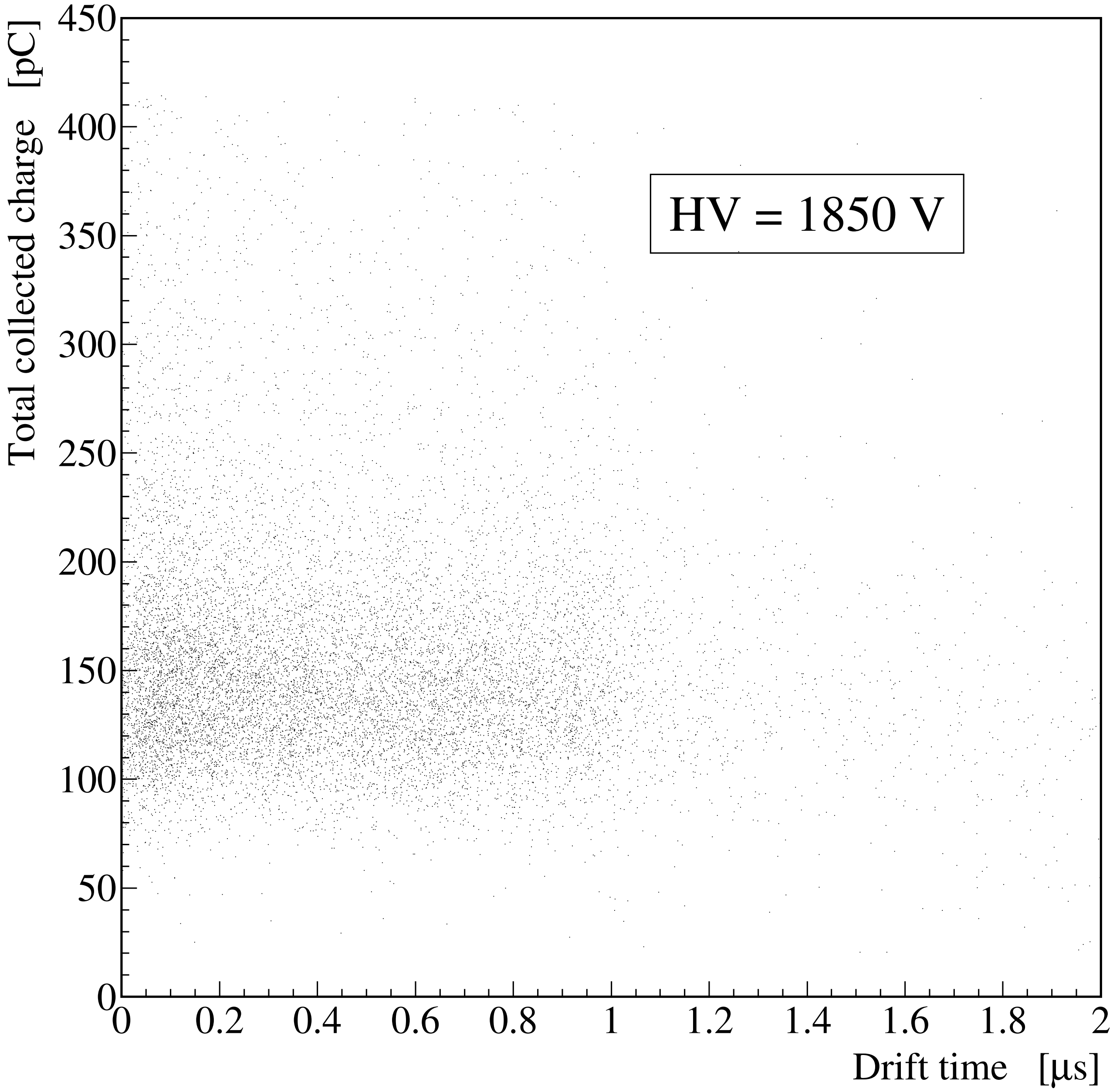


**Fig. 2:** *Total collected charge vs. arrival time of the first electron.*

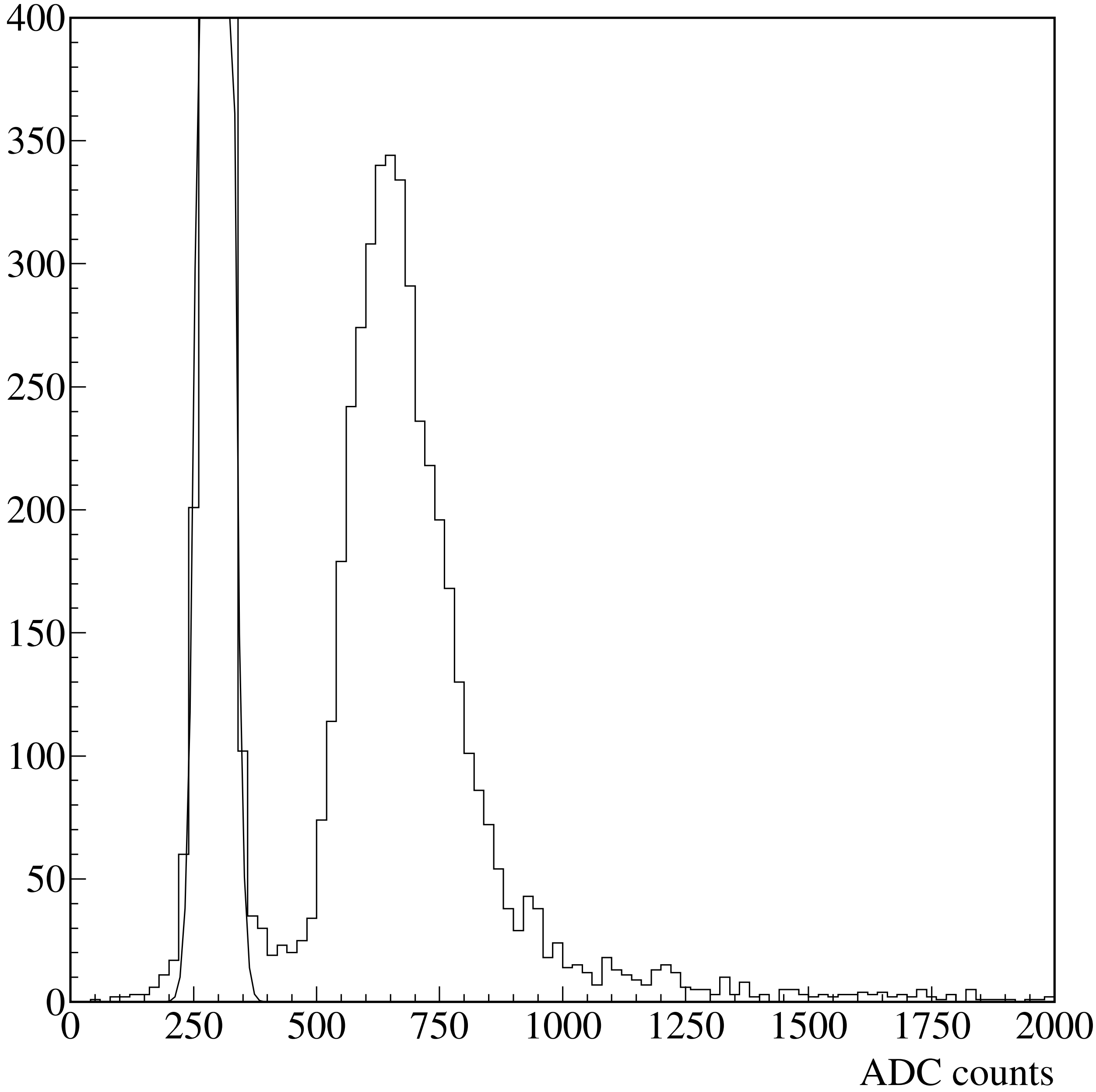


**Fig. 3:** *A typical raw ADC spectrum. The operating voltage was 1,800 V.*

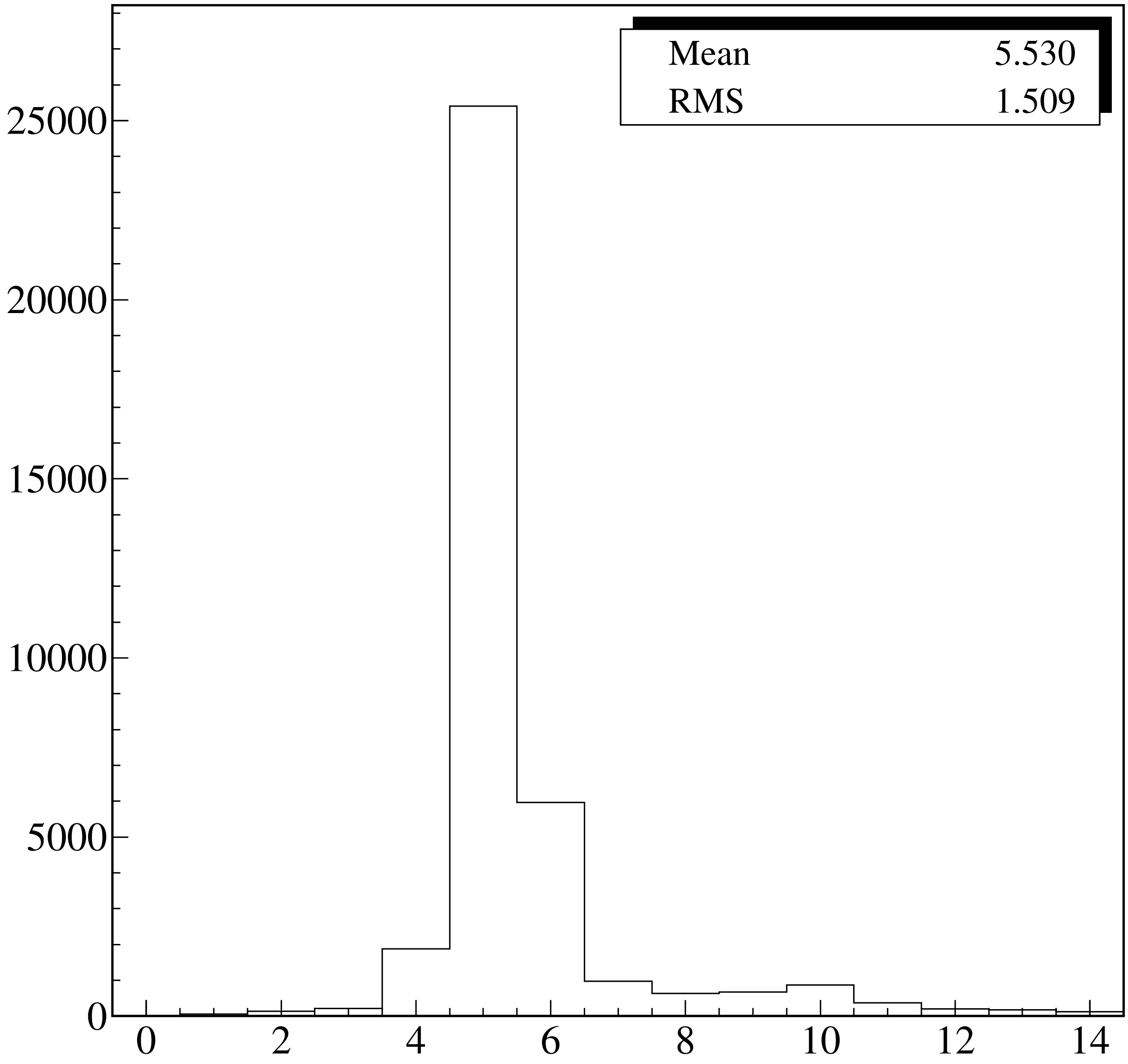


**Fig. 4:** *Multiplicity of hit cells.*

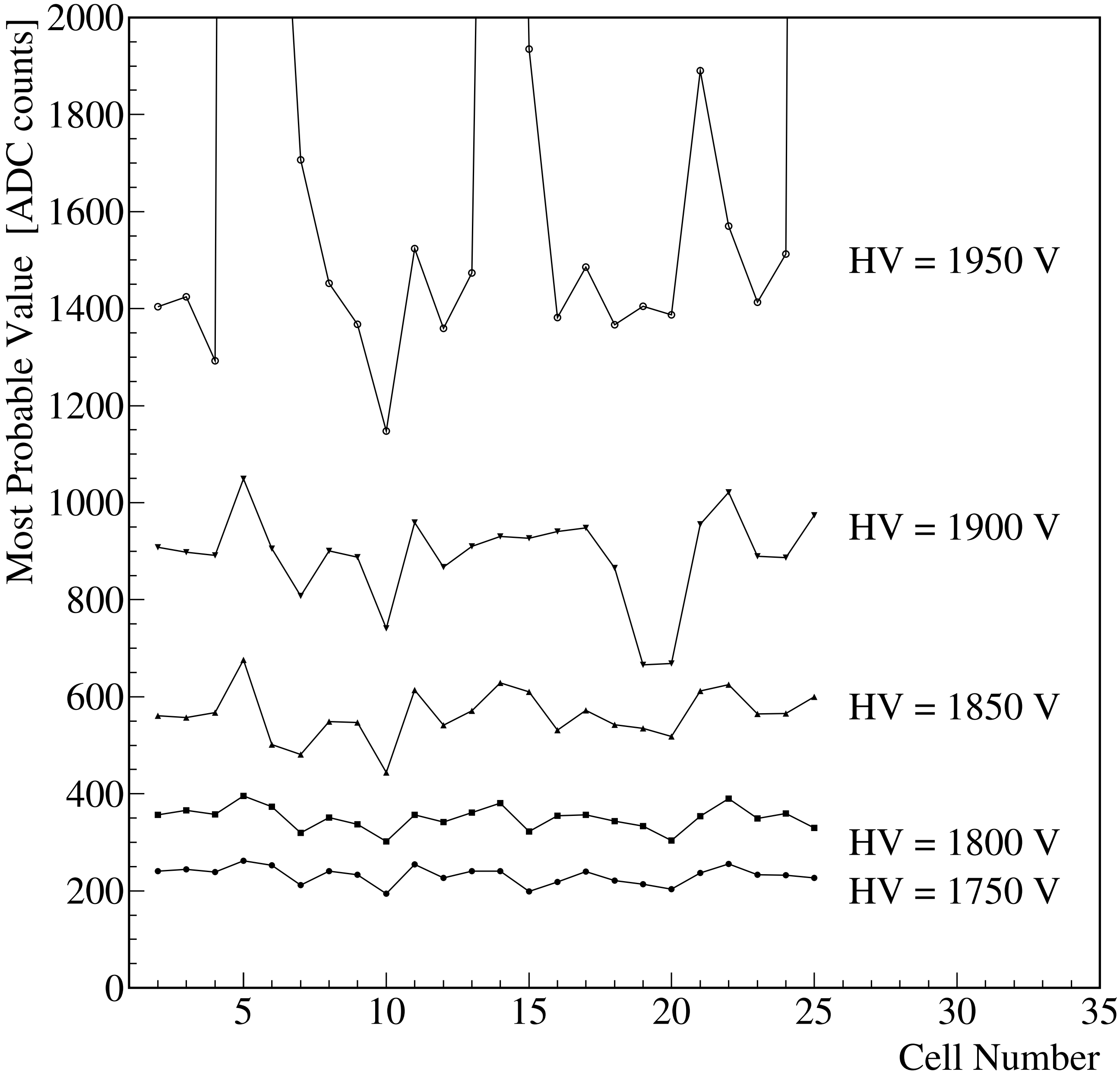


**Fig. 5:** *Most probable values of the pulse height distribution in the cells used in the TM analysis.*

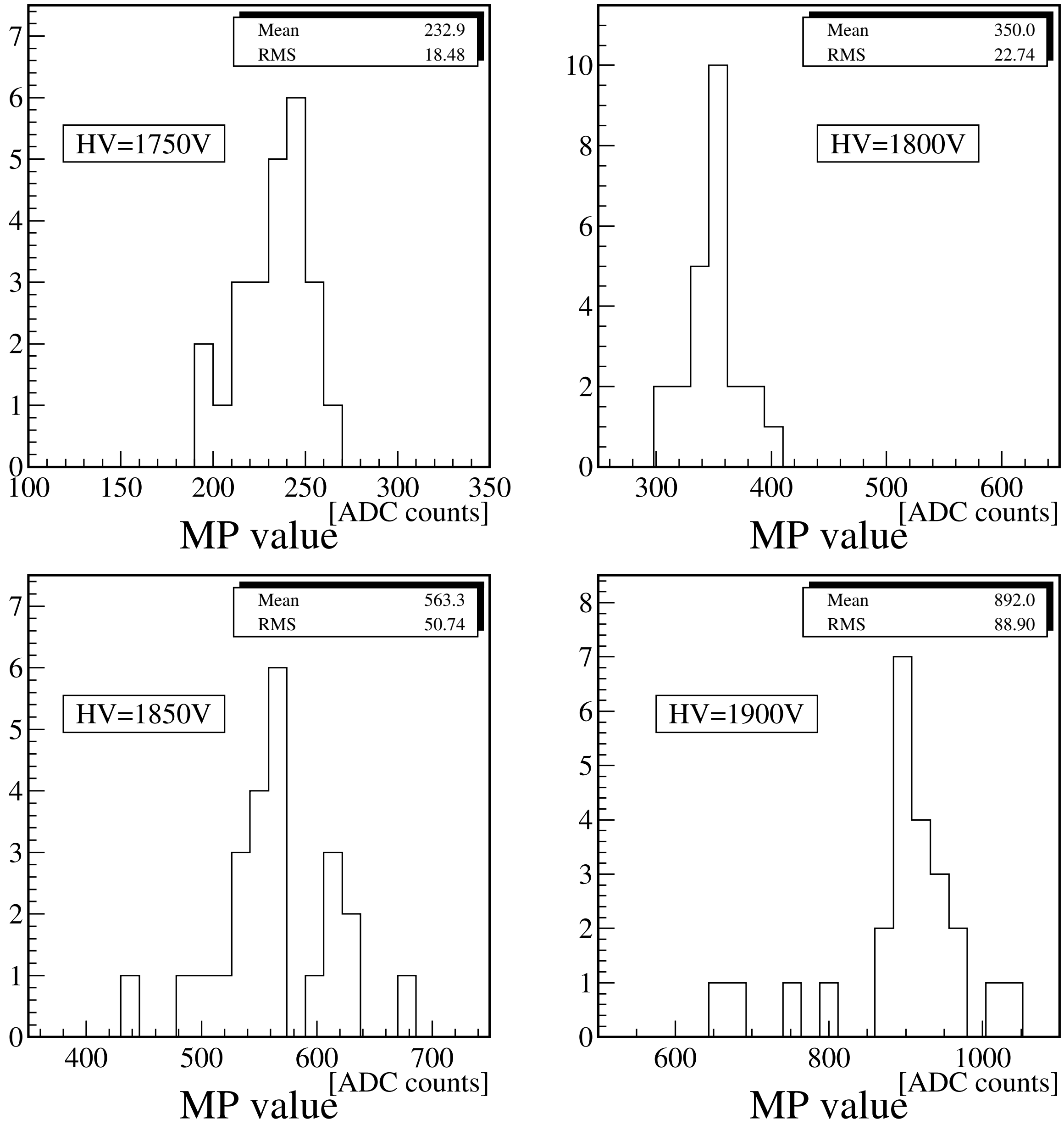


**Fig. 6:** *Histogram of the cells' most probable pulse height for several operating voltages.*

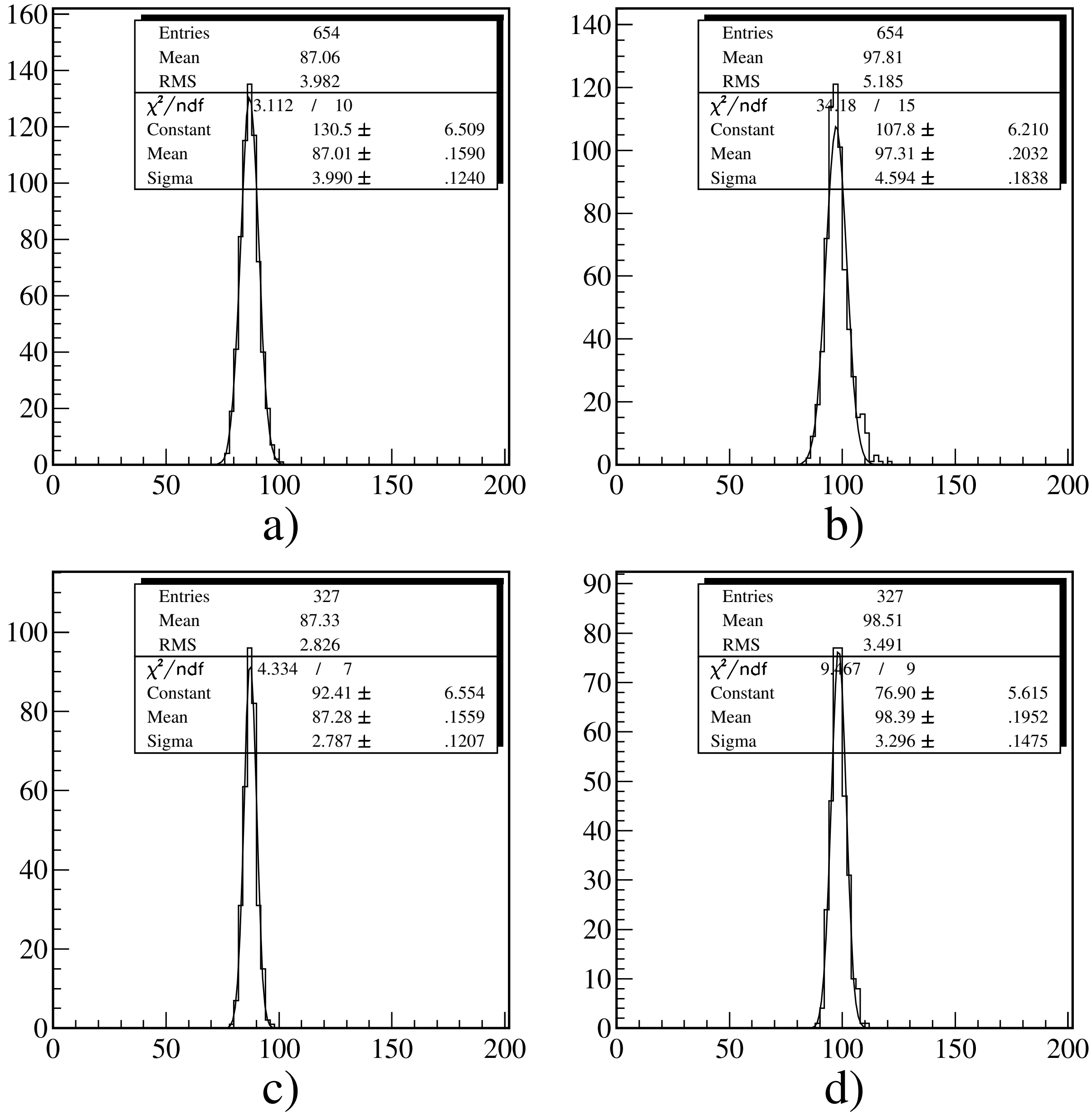


**Fig. 7:** *Examples of Truncated Mean distributions for different values of* $\mathcal{N}$ *and* $f_{\rm acc}$*; a)* $\mathcal{N}$*=50,* $f_{\rm acc}$*=75%; b)* $\mathcal{N}$*=50,* $f_{\rm acc}$*=95%; c)* $\mathcal{N}$*=100,* $f_{\rm acc}$*=75%; d)* $\mathcal{N}$*=100,* $f_{\rm acc}$*=95%.*

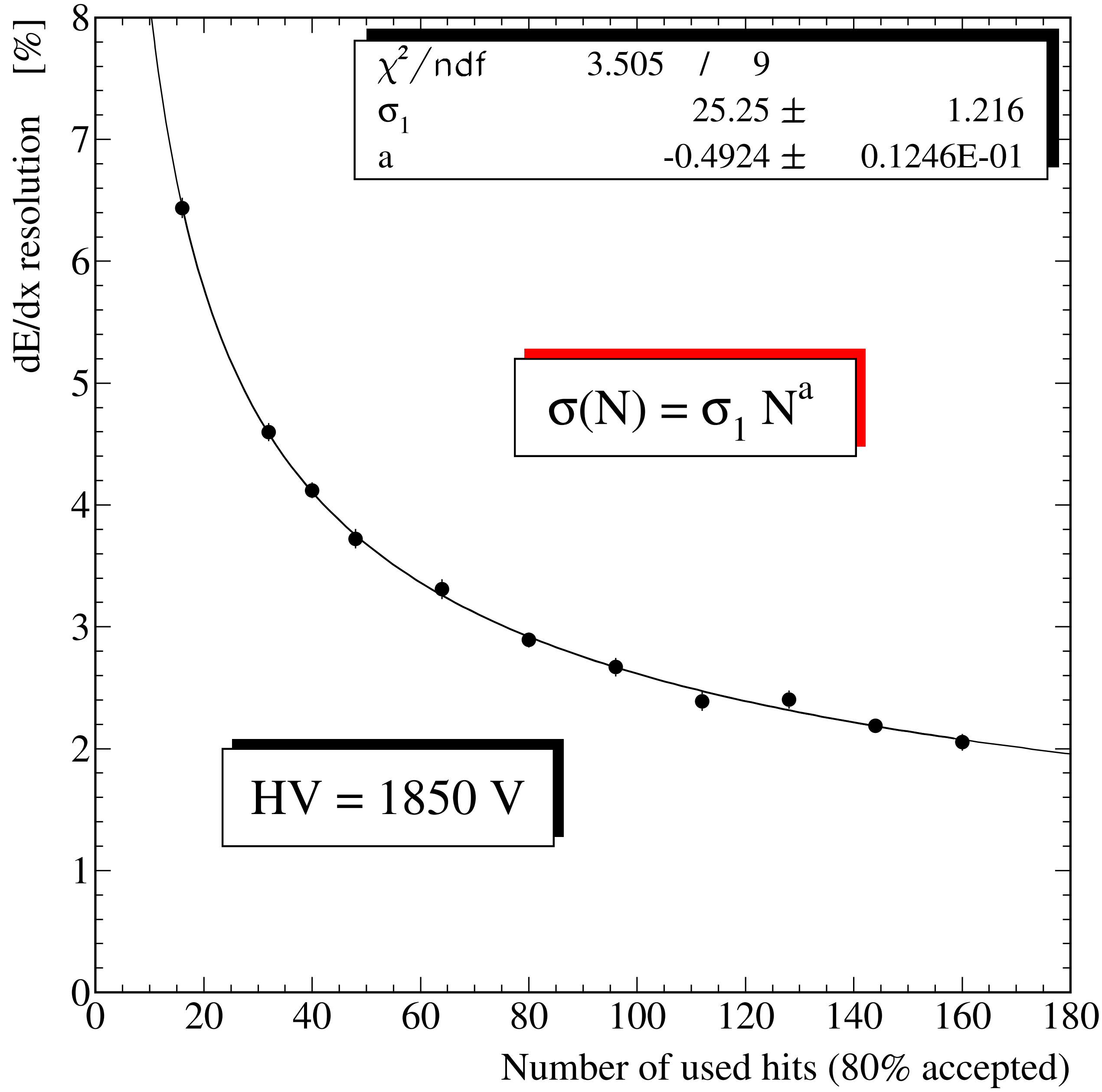


**Fig. 8:** *d$E$/d$x$ resolution vs. number of hits used in the truncated mean, in the case HV=1,850 V, $f_{\rm acc}$=80%. The curve is the result of the fit with the function $\sigma_{{\rm d}E/{\rm d}x}(N) = \sigma_1 \cdot N^a$.*

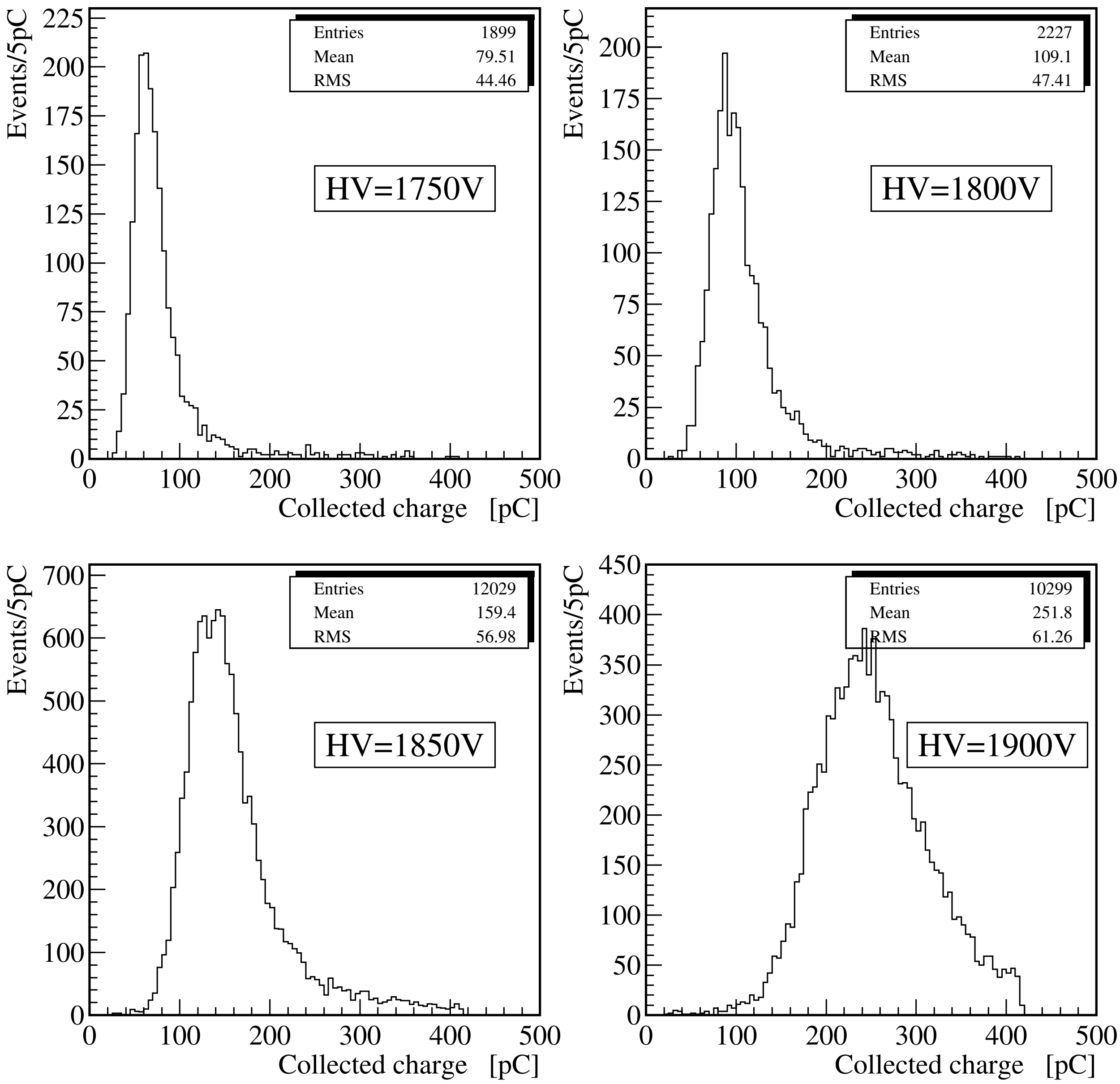


**Fig. 9:** *ADC spectra for several operating voltages.*

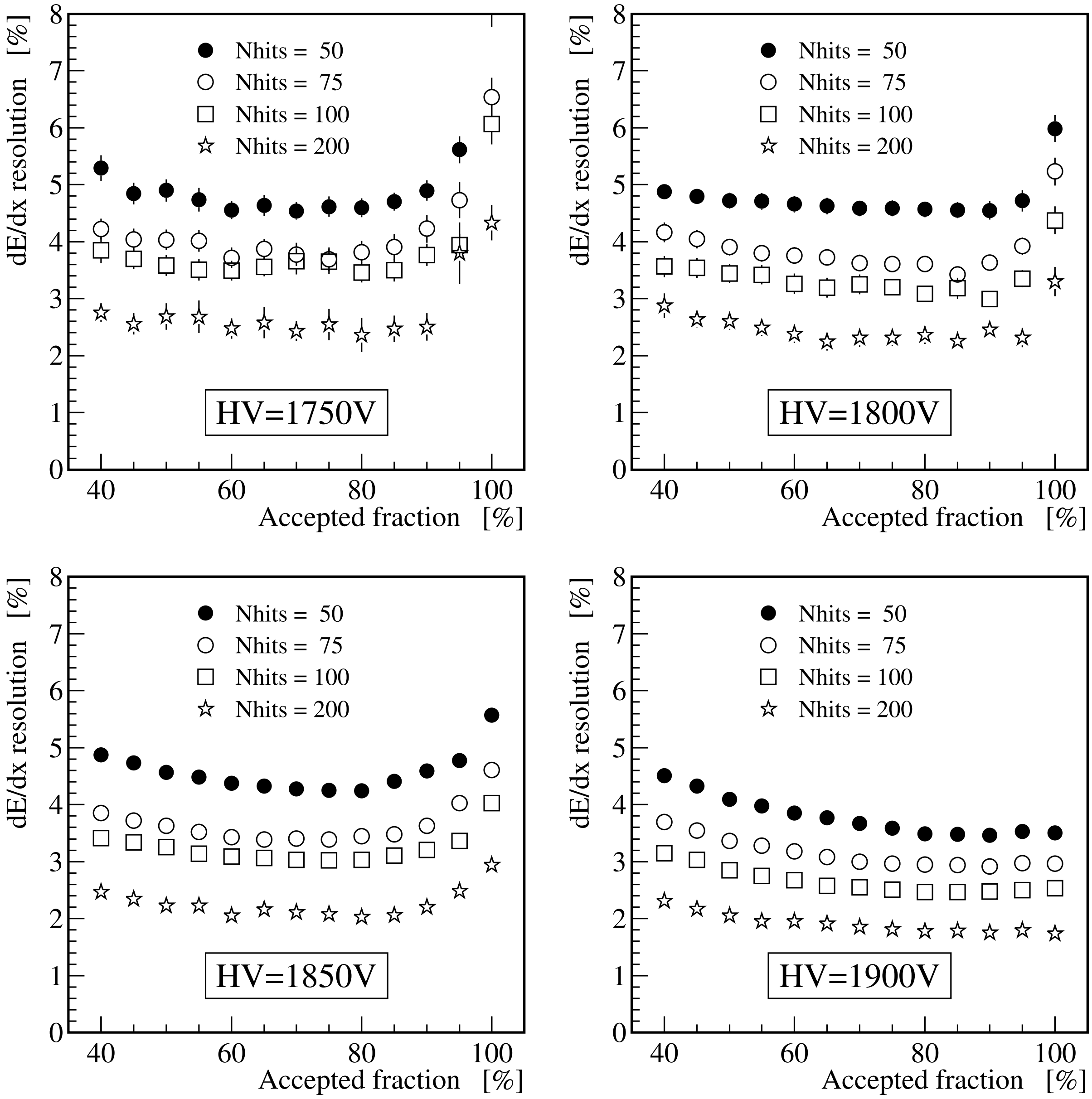


**Fig. 10:** $\mathrm{d}E/\mathrm{d}x$ *resolution vs.* $f_{\mathrm{acc}}$ *for different* $\mathcal{N}$ *values and operating voltages.*

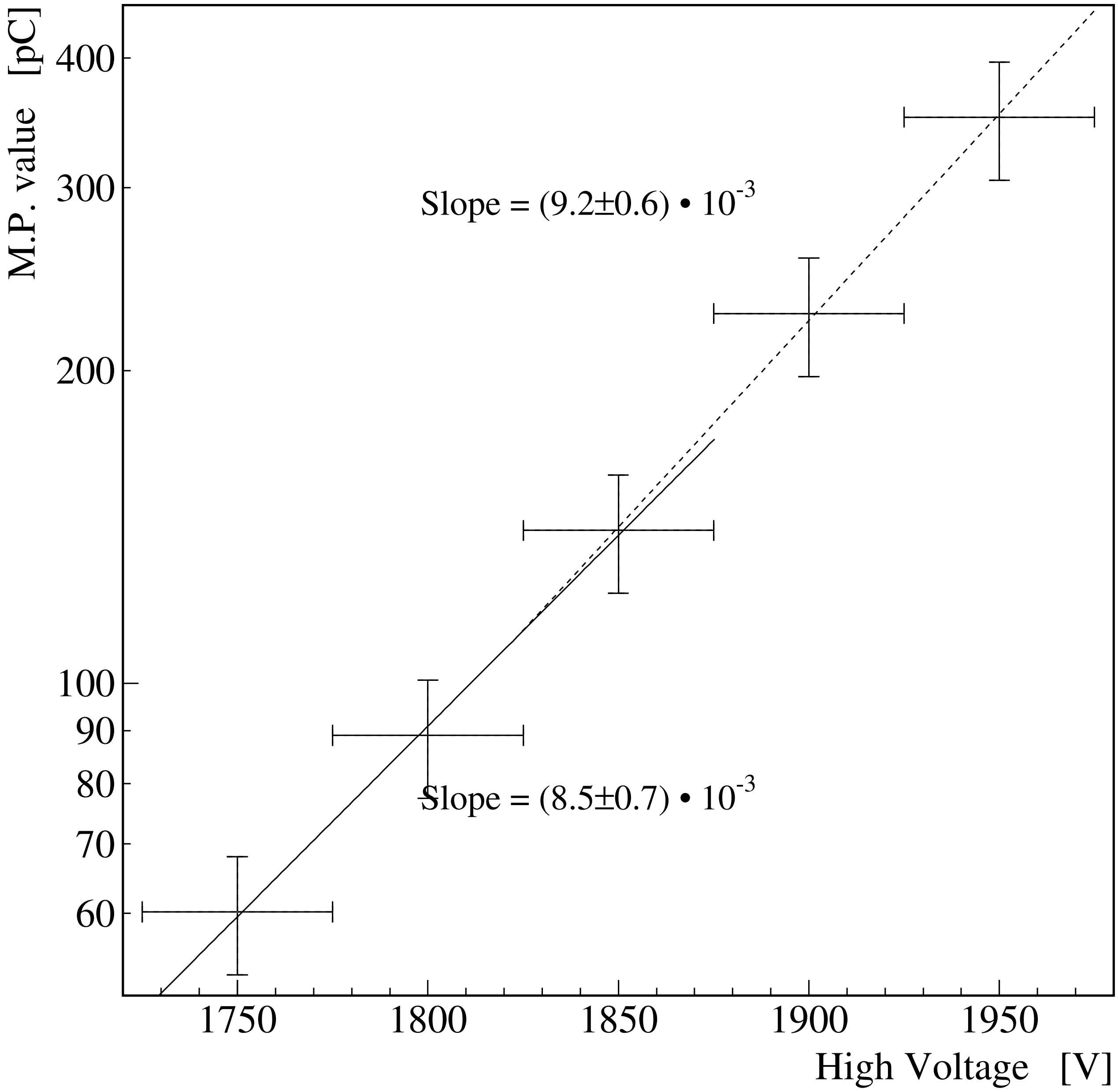


**Fig. 11:** *Most probable value of the pulse height distribution vs. operating voltage.*

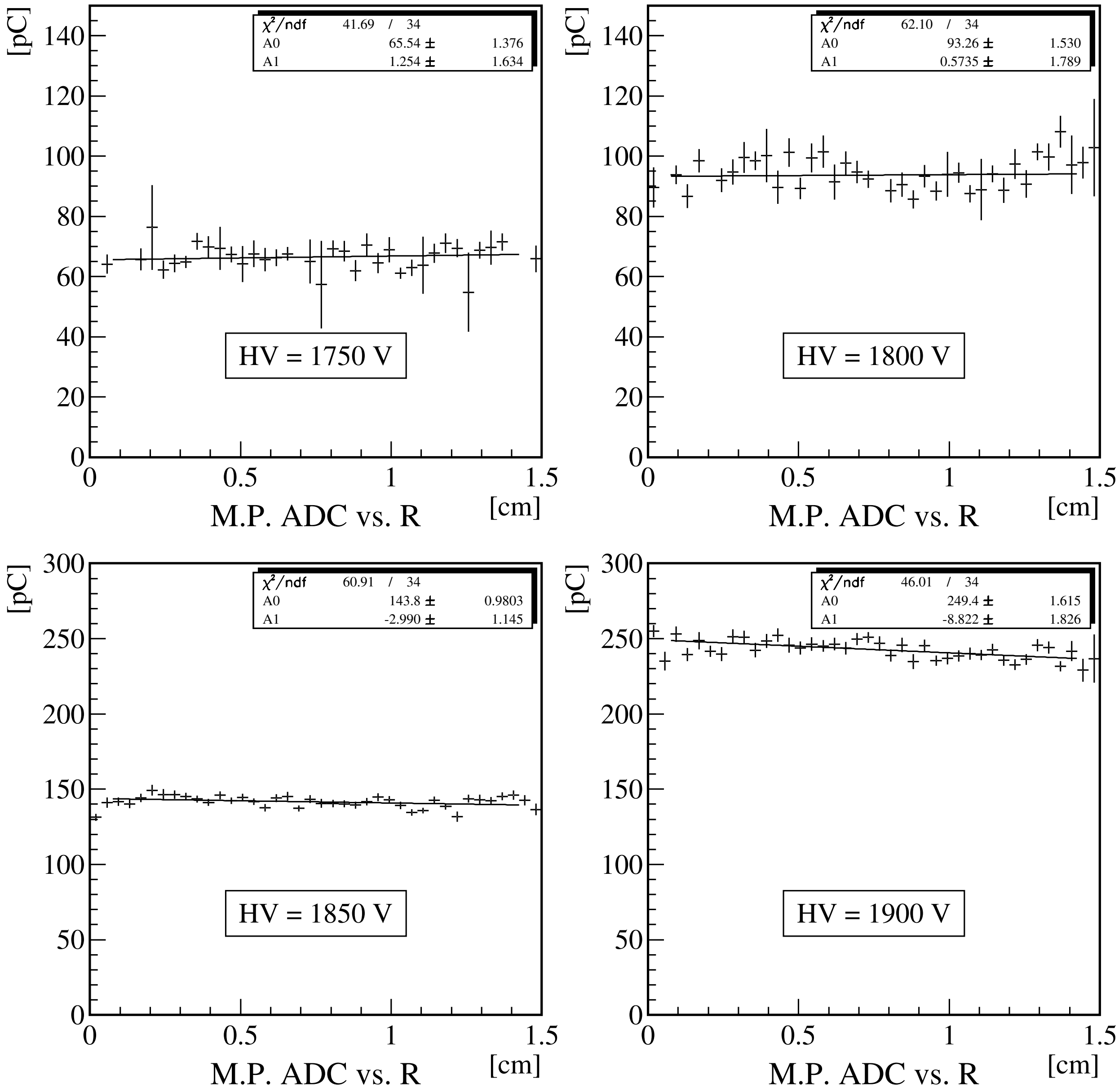


**Fig. 12:** *Profile of collected charge vs. drift distance.*

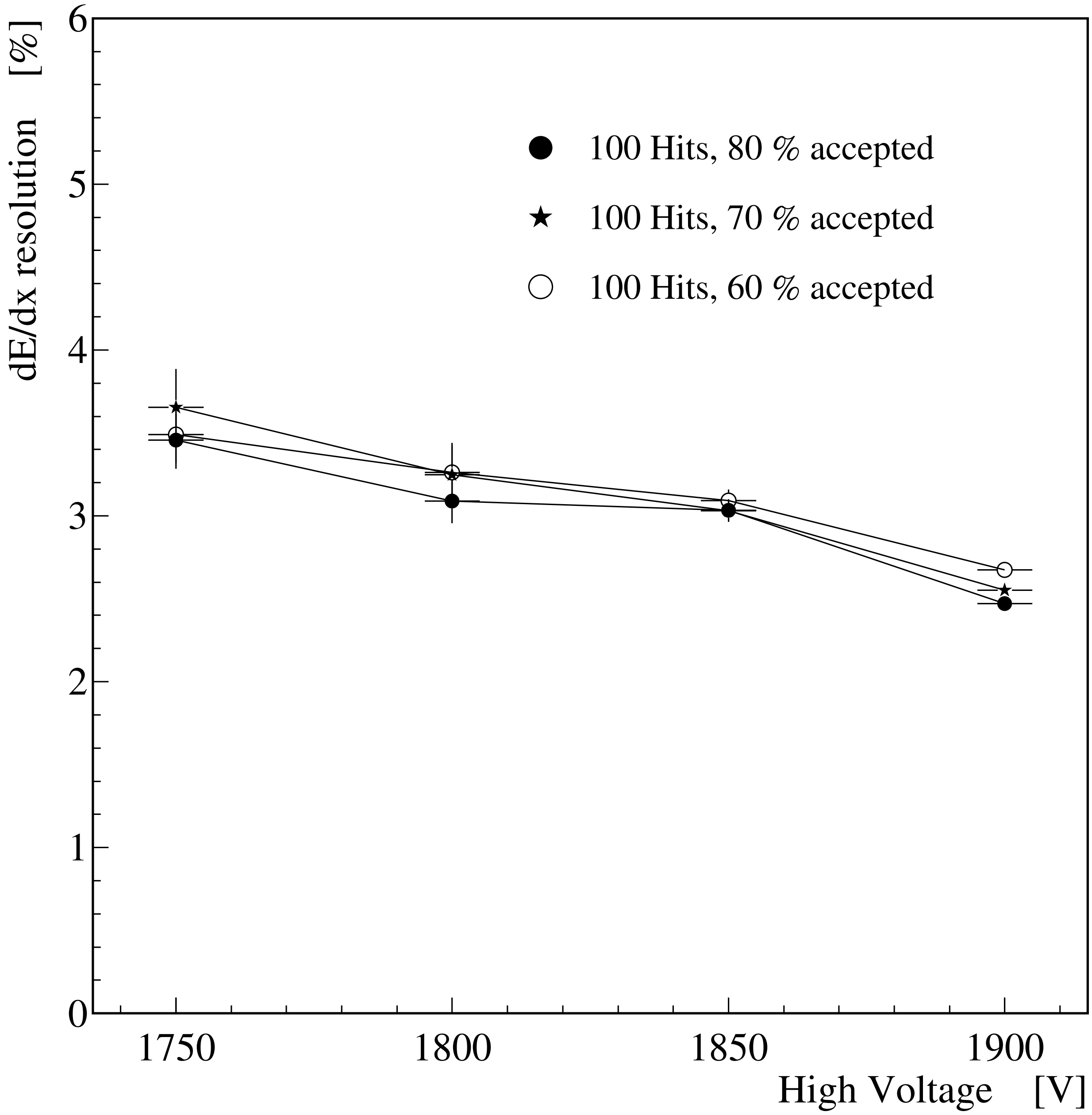


**Fig. 13:** d$E$/d$x$ *resolution vs. operating voltage.*

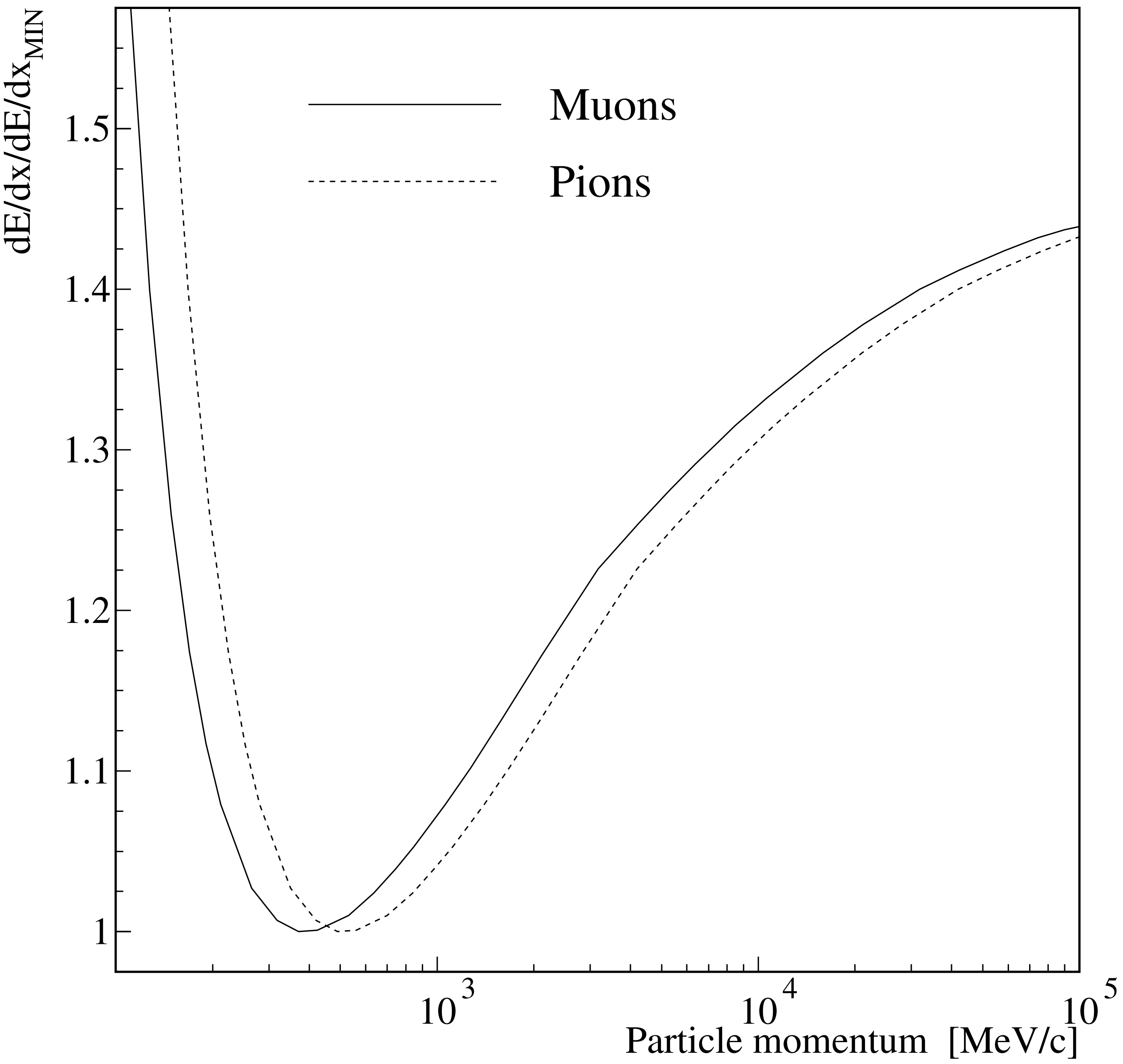


**Fig. 14:** d$E$/d$x$ *curves in* 90%He−10%$i$C$_4$H$_{10}$.

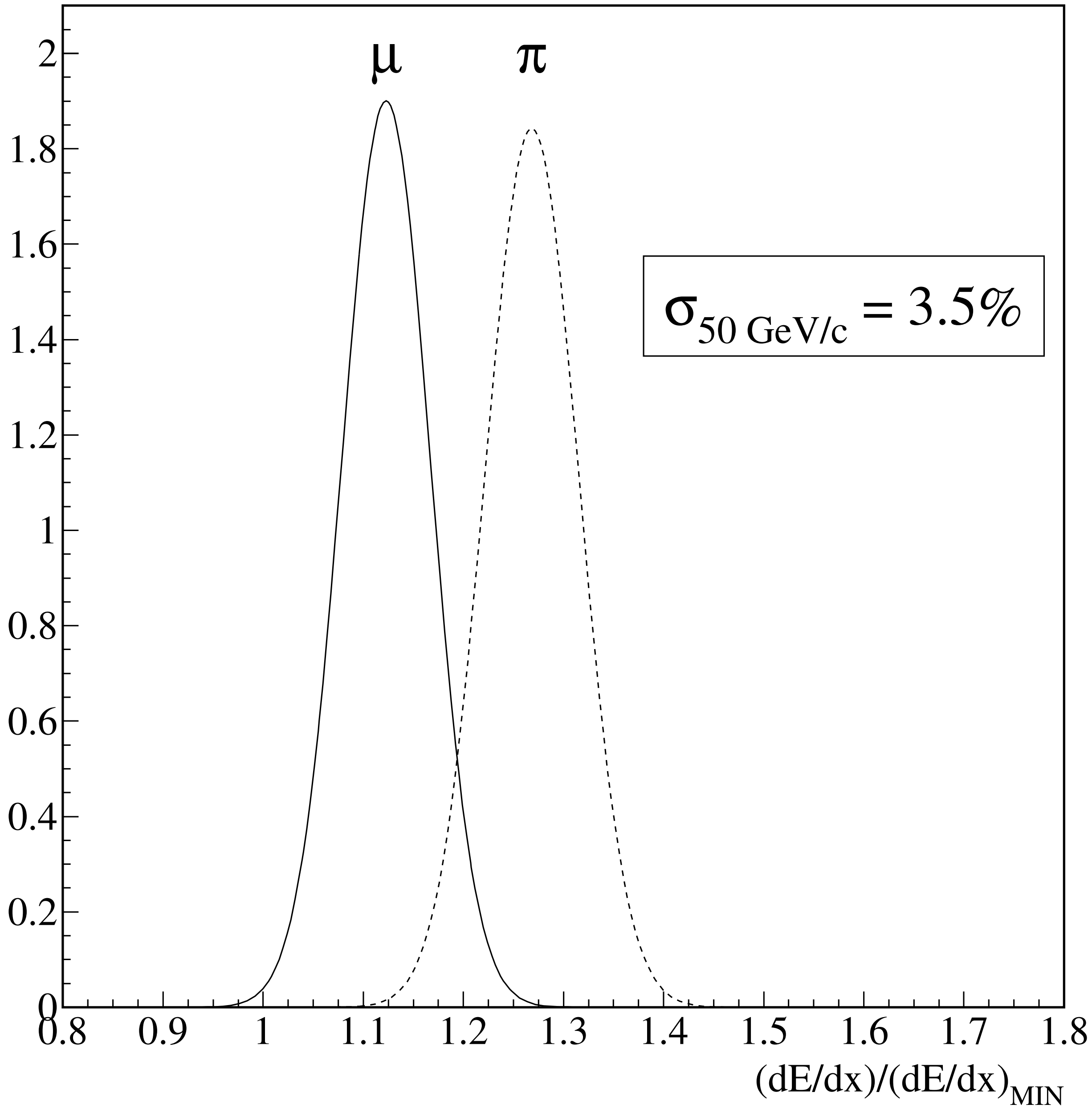


**Fig. 15:** *Calculated shapes of the TM distribution at* $p = 200\,\mathrm{MeV}/c$.

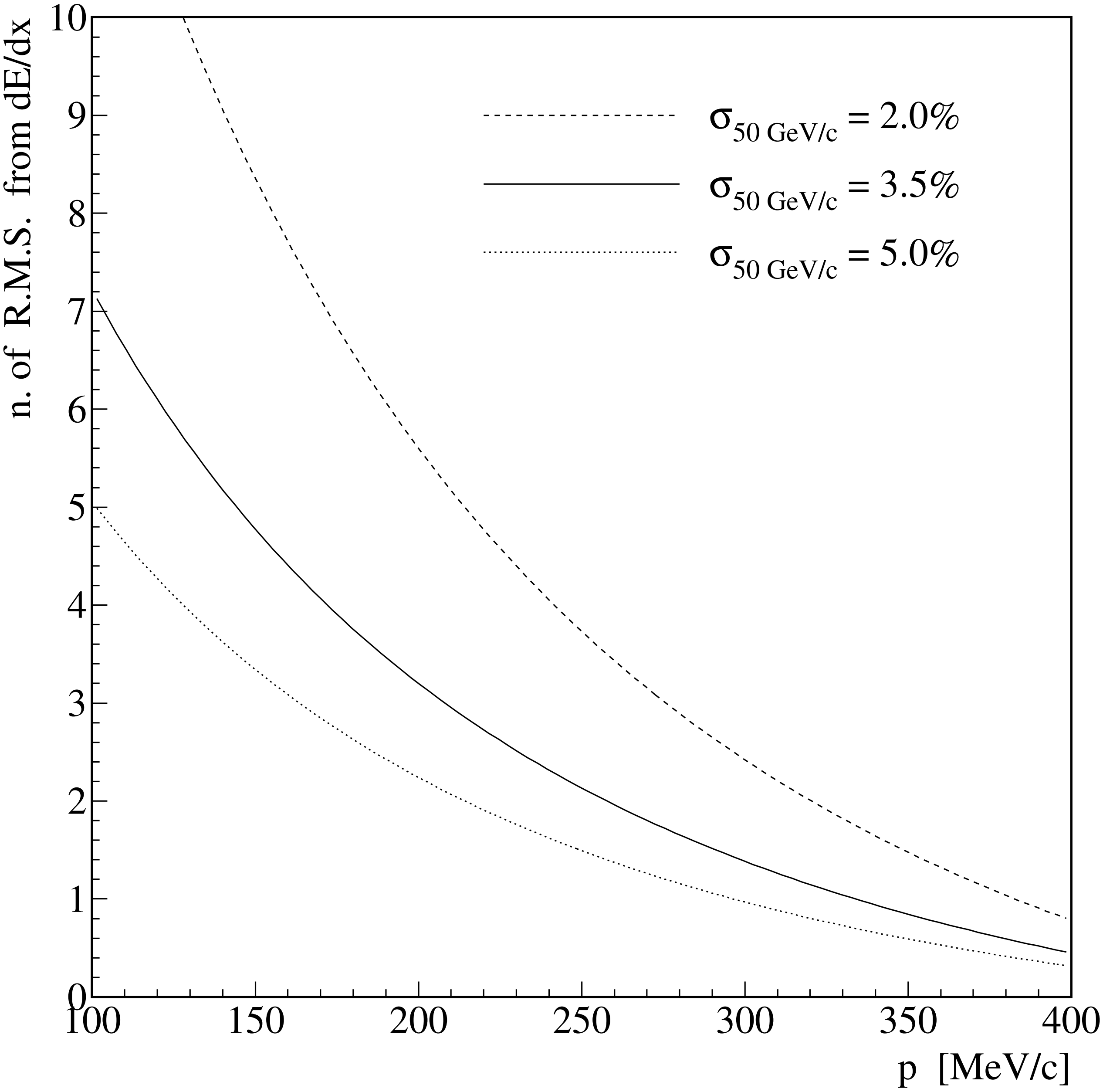


**Fig. 16:** *Number of R.M.S. separating the muon and the pion peaks.*

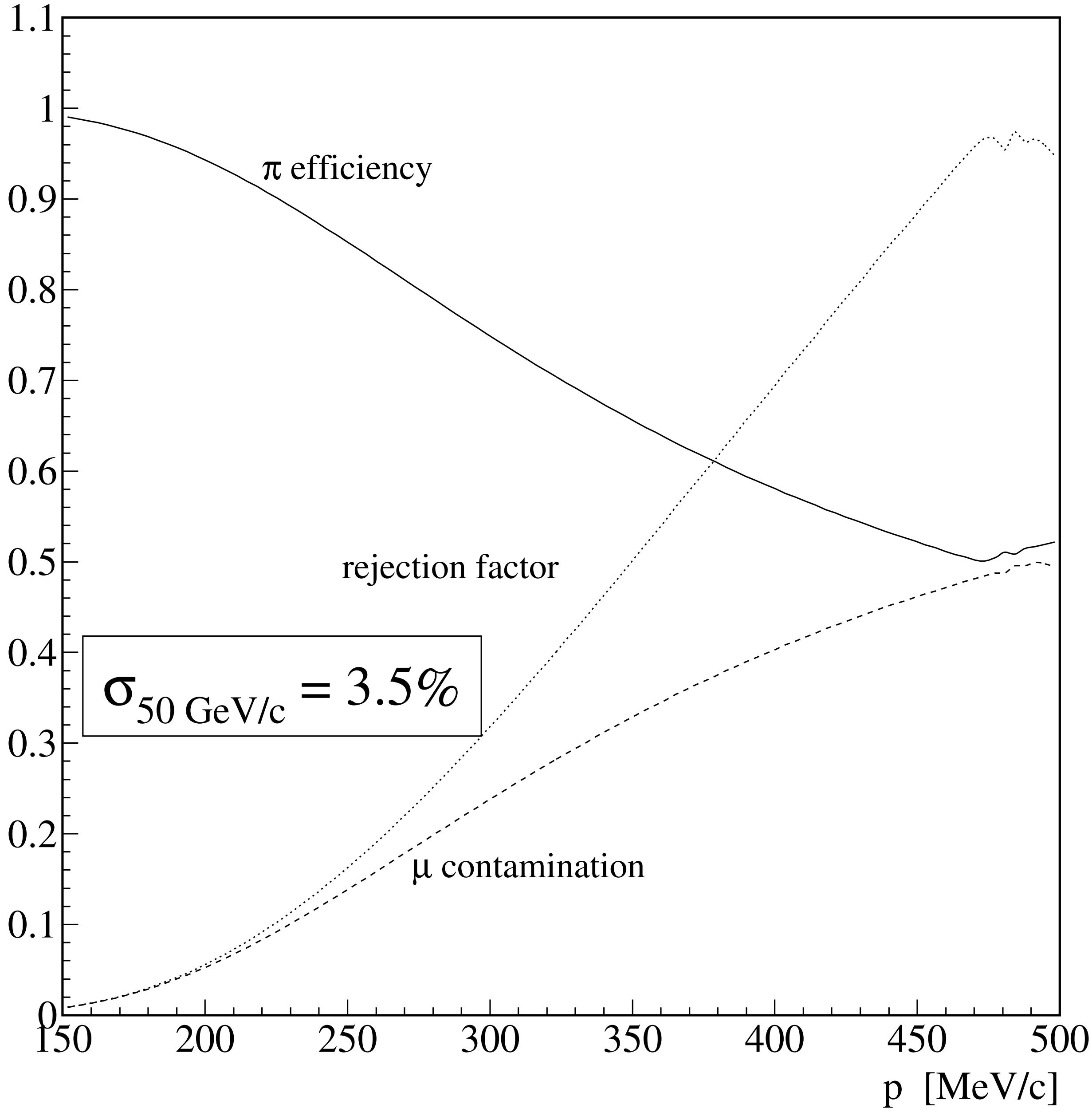


**Fig. 17:** *Pion and muon efficiencies and rejection factor cutting the TM signal exactly halfway between the two peaks.*

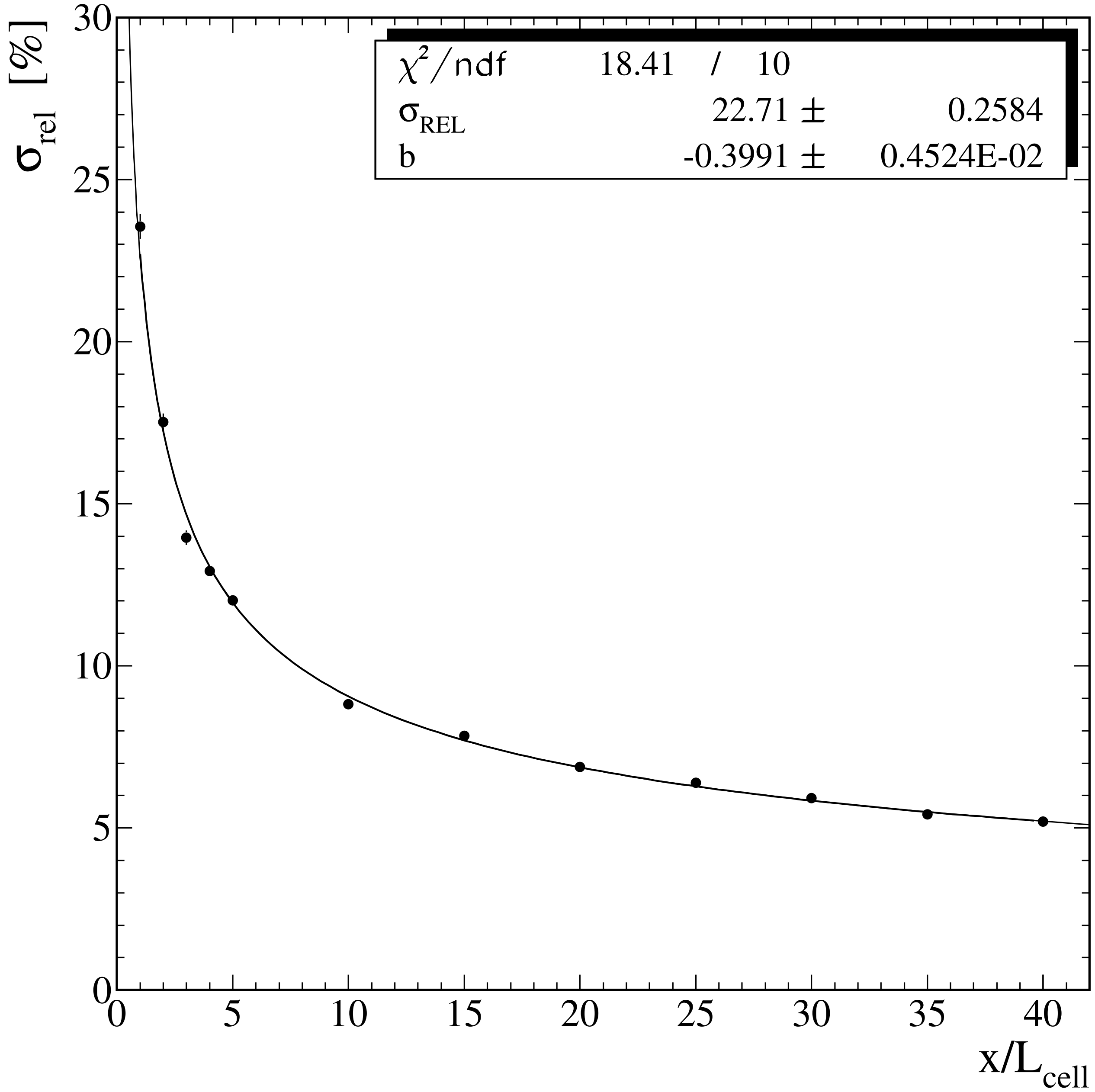


**Fig. 18:** *Relative width of the single supercell pulse height distributions, as a function of the supercell length.*

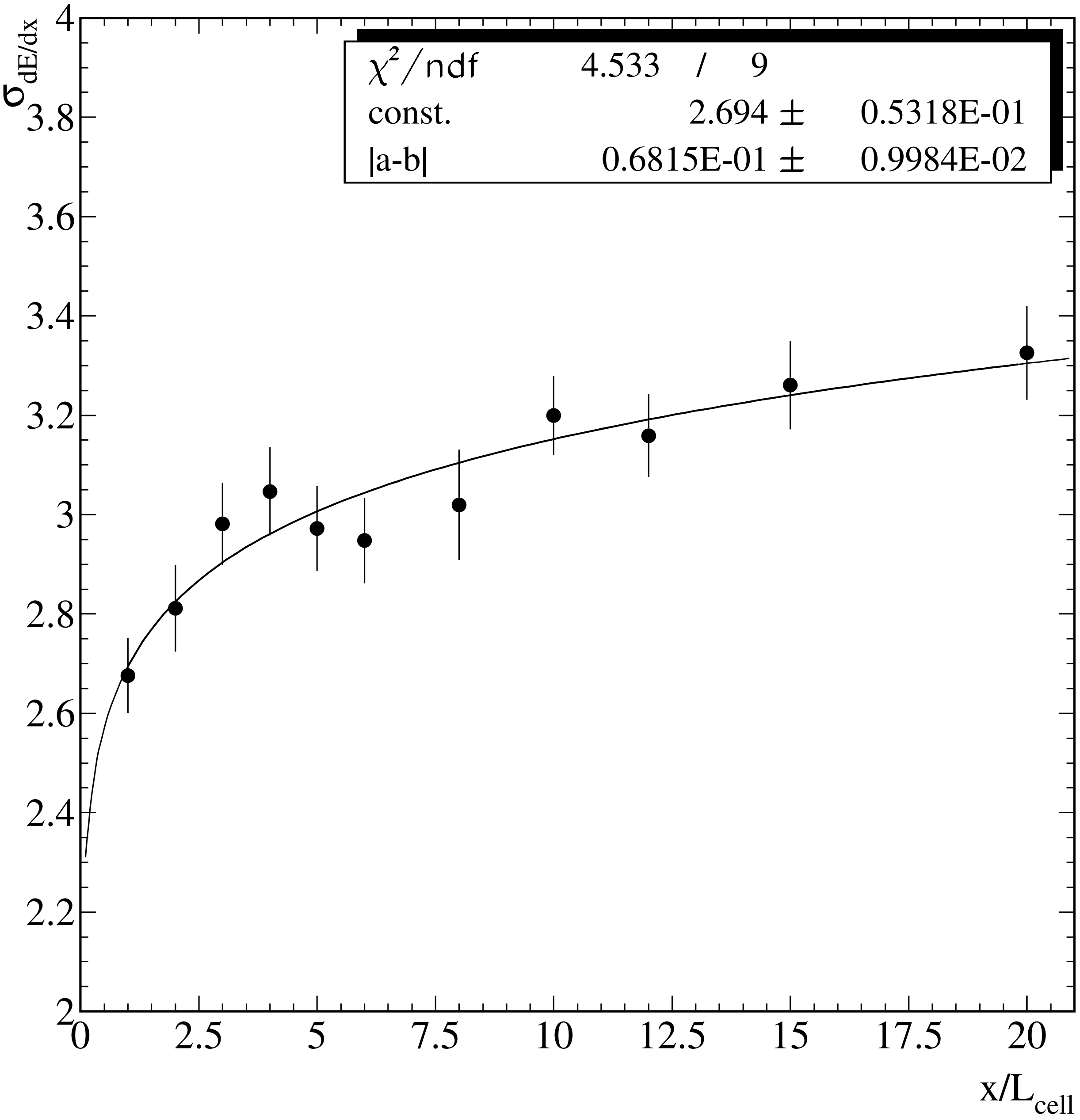


**Fig. 19:** *TM resolution vs. supercell length.*